JOURNAL OF SPACECRAFT AND ROCKETS
Vol. 35, No. 3, May–June 1998

Fin Damage and Mass Offset for Kinetic Energy Projectile Spin/Pitch Lock-In

Ameer G. Mikhail*
U.S. Army Research Laboratory, Aberdeen Proving Ground, Maryland 21005-5066

A study and a general model for the roll/pitch frequency lock-in phenomenon are made for long antitank kinetic energy projectiles and missiles in general to quantify the necessary projectile damage/defect required to cause the lock-in. Fin damage and body mass offset are modeled as the forcing forces and moments (asymmetries) causing the lock-in. Idealized fin damage is modeled. The corresponding pitch, side-slip, and roll equations are numerically integrated. The nonlinear induced roll moment is essential in coupling the pitching/yawing motions with that of the roll motion. A specific and complete projectile case study is presented, in which quantified fin damage and rod mass offset are found to cause such lock-in. Computed flight motion history (pitch, side slip, and roll) and the yaw amplification factor provide insight into this lock-in behavior. The model is general and can be applied to any finned projectile or missile.

Nomenclature

A_d = damaged area of a fin panel, in.^{2}
A_f = area for one single fin panel, in.^{2}
A_{ref} = reference area ($\pi d^2/4$), in.^{2}
C_D = drag coefficient, drag force/$(0.5\rho_\infty V_\infty^2 A_{\text{ref}})$
C_l = rolling moment coefficient, $l/(q_\infty A_{\text{ref}} d)$
C_{li} = induced roll moment coefficient; Eq. (1)
C_{lp} = roll moment damping coefficient derivative, $\partial C_l/\partial(pd/V)$, per radian
$C_{l\delta}$ = fin produced roll moment coefficient derivative, $\partial C_l/\partial\delta$, per radian
C_M = pitching moment coefficient, pitching moment (about the mass center)/$(q_\infty A_{\text{ref}} d)$
$C_{Mp\alpha}$ = Magnus moment slope coefficient, Magnus moment/$(q A_{\text{ref}} d(pd/V)\alpha)$
$C_{Mq} + C_{M\dot{\alpha}}$ = pitch moment damping coefficient, pitch damping moment/$(q A_{\text{ref}} d(\hat{q}d/V))$
$C_{M\alpha}$ = pitching moment slope coefficient, $\partial C_M/\partial\alpha$, per radian
C_{M0} = asymmetry pitching moment coefficient
C_N = normal force coefficient, normal force/$(q_\infty A_{\text{ref}})$
$C_{N\alpha}$ = normal force slope coefficient, $\partial C_N/\partial\alpha$, per radian
d = projectile reference diameter, in.
I_x = axial (polar) moment of inertia about the body spin axis, lb-in.^{2}
I_y = transverse moment of inertia about an axis passing through the body center of mass, lb-in.^{2}
L = total length of the projectile, in.
l = roll moment, lb-in.
M = Mach number of the projectile
m = mass of projectile
n = number of fins in a fin set
n_d = number of damaged fins in a fin set
p = spin rate of projectile, rad/s (except where otherwise noted in Hz)
$\hat{q}$ = local pitching rate, rad/s
q_∞ = dynamic pressure $(0.5\rho V^2)$, psi
V = projectile velocity, ft/s
α = body pitching angle of attack, deg
$\dot{\alpha}$ = $\mathrm{d}\alpha/\mathrm{d}t$
α_t = total angle of attack (yaw) ($\sqrt{(\alpha^2+\beta^2)}$), deg
β = body side-slip angle of attack, deg
Γ = initial angle of mass offset location, deg
γ = fin plane roll orientation angle with respect to the plane of angle of attack, deg
Δcg = mass offset radial distance from body center, in.
Δt = time step for numerical integration, s
$\Delta_1, \Delta_2, \Delta_3$ = fin damage parameters: deg, deg, and in., respectively
δ_d = design value of the fin cant angle, deg
δ_{dg} = value of the fin cant damage angle, deg
δ_{eq} = equivalent fin cant angle for a whole fin panel for the partially canted (chamfered) fin, deg
$\delta_1, \delta_2, \delta_3$ = angles of the damaged area of the fin panel, deg
λ = angle of the C_{M0} asymmetry moment, deg
ρ = air density, slug/ft^3
ϕ = roll angle, measured from a fixed reference plane, rad
$\dot{\phi}$ = roll (spin) rate, $\mathrm{d}\phi/\mathrm{d}t$, rad/s (except otherwise noted in Hz)
$\bar{\phi}$ = $(\phi + \phi_0 - \hat{\phi})$
$\hat{\phi}$ = pitching motion plane, measured from same reference plane, $\tan^{-1}(\beta/\alpha)$
ϕ_0 = initial roll angle, measured from same reference plane
ω_n = first natural frequency in lateral bending, rad/s
ω_p = pitching motion frequency, $\sqrt{(-C_{M\alpha} q A_{\text{ref}} d/Iy)}$, rad/s

Introduction

LONG antitank kinetic energy (KE) projectiles and also missiles are known to occasionally exhibit an abnormal flight behavior characterized by 1) spinning at a different rate than their intended design values and 2) having larger-than-expected yawing motion angles. In a few cases, this behavior can be catastrophic to the motion and mission of the vehicle, causing ineffective armor penetration for the KE projectile case or uncontrollable flight for the missile case. Note that the projectile flight duration is only 1–3 s.

When these two observations occur, it is most likely that a roll/pitching motion lock-in had occurred where the vehicle was unintentionally spun, due to damaged fins or some other reasons, close to the pitching motion frequency of the vehicle. These fin damages are usually referred to in the literature as asymmetries that are suffered by the vehicle. Figure 1 shows a fin impact imprint indicating damaged parts of two fins,[1] bent by angles in excess of 30 deg, and a KE projectile impact imprint[2] at 10,000 ft indicating large yaw angle, estimated here at about 8.8 deg.

Presented as Paper 96-3448 at the AIAA Atmospheric Flight Mechanics Conference, San Diego, CA, July 29–31, 1996; received Aug. 5, 1997; revision received Jan. 9, 1998; accepted for publication Jan. 12, 1998.

*Aerospace Engineer, Propulsion and Flight Division, Weapons Technology and Materials Research Directorate. Associate Fellow AIAA.

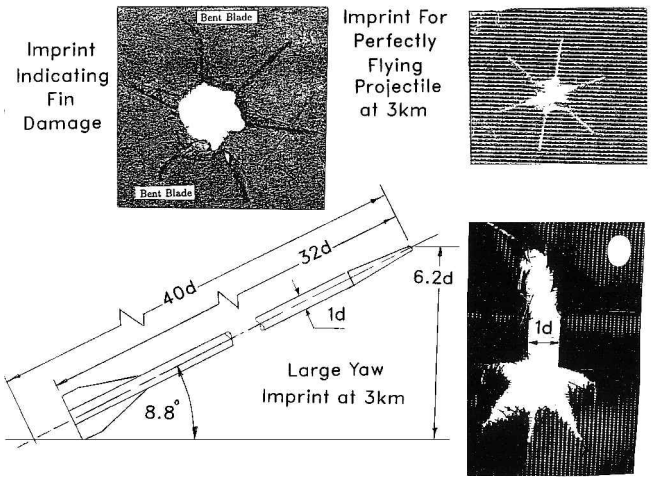

Fig. 1 Observed damaged fins and large yaw for a generic KE projectile; dimensions in caliber.

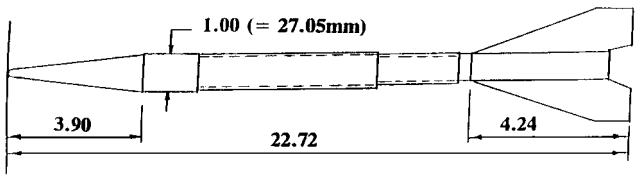

Fig. 2 Geometry of the 120-mm M829 subcaliber KE projectile.

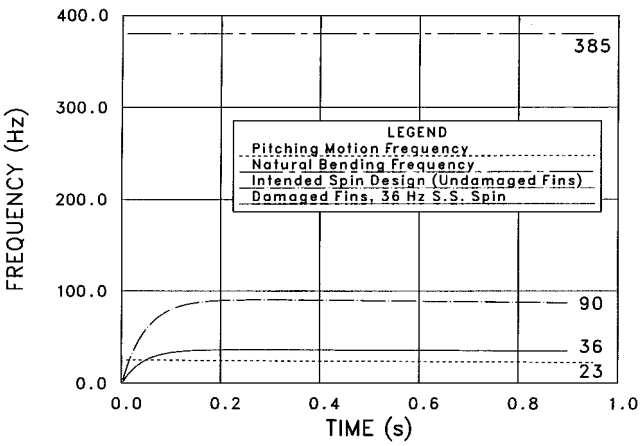

Fig. 3 Design spin (undamaged fins) falling between the two limiting frequencies; 120-mm M829 KE projectile (steel).

This roll/pitch lock-in phenomenon is not new and has been studied by many researchers since the late 1940s. Nicolaides[3] provided an early analysis whereas Price[4] provided a useful and practical model for the mechanisms causing the phenomenon. Clare[5,6] provided the effect of nonlinearities on such motion. Murphy[7] included the asymmetries in his formulation and later showed[8] that lock-in can happen at a reverse spin rate. More recently, Lin et al.[9] studied this problem for a re-entry vehicle (with no fins) and considered longitudinal body curvature due to flexure as part of the total angle of attack, in a zeroth-order model for flexure effects. For earlier studies, the reader is referred to Refs. 4, 5, 8, and 9, which together list about 186 references covering this lock-in behavior and its model development over the years.

The design spin for a KE projectile or a missile has to avoid being close to the natural pitching motion frequency or to the first natural lateral bending frequency of the vehicle. For the KE projectile shown in Fig. 2, the former is about 24 Hz (decreases from 25 to 23), whereas the latter (for the steel model herein) is about 385 Hz. The design spin for that projectile is 90 Hz, as shown in Fig. 3. Certain fin damage can cause the projectile to underspin its design value to near its pitching frequency, as shown in Fig. 4. These particular

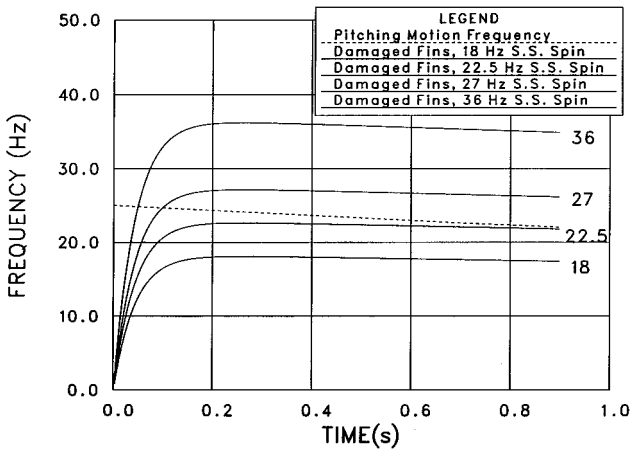

Fig. 4 Spin cases studied near the pitching frequency (undamaged fins); 120-mm M829 KE projectile (steel).

spin values near this pitching motion frequency will be studied in detail later in this work. In Ref. 10, the spin lock-in with the upper frequency limit (the first bending frequency) due to structural causes was studied and reported. In the present lock-in phenomenon, the mechanisms for causes are dynamic-motion related to the pitching and side-slip angles coupled to a lower roll rate due to fin damage. The present study deals with the lock-in at this lower limit, its implication, and the motion instability amplification it induces. Reference 11 provides results for pitch lock-in with rod flexure, but gives no details about the exact formulation, equations, or roll information, including any induced roll moment.

Usually, roll implies a low spin value. Historically it came from the aeronautical reference to aircraft roll rate. Spin, however, indicates high value of roll. Commercial aircraft may roll only few degrees to bank, whereas a military aircraft may do few complete rolls for maneuver. Missiles usually have low roll rate (1–5 Hz), whereas finned projectiles spin at 50–150 Hz and unfinned projectiles may be spun to over 300 Hz. In the present work, the spin/pitch lock-in will be occasionally called roll/pitch lock-in, as it is frequently called in the literature.

The present work adapts the work of Price[4] to the formulation of Ref. 7. Numerical solutions will be obtained for the three coupled roll/pitch/side-slip equations. A case study will be made for the 120-mm M829 steel version of the projectile. Flight histories and impact imprints will be presented under different fin damage and mass offset values.

Analysis

Definitions

Resonance between the roll and pitching frequencies is defined as when the former is affected by the value of latter when the two values match each other. Roll lock-in is when the former frequency attains and maintains the value of the latter for long and persistent time (1–3 s for KE projectiles, many seconds or minutes for a missile). Vehicles can roll resonate when crossing the pitching frequency but may not lock-in to it. Vehicles that roll lock-in must resonate with the pitch frequency. Lock-in is a persistent resonance for the flight duration of the vehicle. However, vehicles may temporarily lock-in but then escape later, in what might be called a prolonged resonance.

Yaw angle is the side-slip angle β. The yawing motion is, therefore, the motion in the yaw plane of that angle. However, it is common in ballistics to refer to the total angle of attack as the yaw angle and the total motion as the yawing motion. In the present work, yaw will refer to the correct side-slip definition.

Induced Roll Moment

The induced roll moment C_{l_I} is generated on a finned vehicle due to the cyclic fin loading at different angles of attack. Its magnitude is function of both the fin orientation angle during roll (with respect to a reference plane) and with the total angle of attack. It is nonlinear (sinusoidal) with the fin orientation angle and nonlinear with the total angle of attack. Reference 4 only cites a case of wind-tunnel

experiment of the Aerobee 150A sounding rocket, but the actual test values themselves were provided in Ref. 5, which provides more details about the analytic form of that coefficient. C_{li} is defined as

$$C_{li} = \frac{\text{induced roll moment}}{(q A_{\text{ref}} d \sin(n\gamma))} \tag{1}$$

Clare[5] provides an analytic (fitted) form based on the experimental testing for the Aerobee rocket:

$$C_{li} = \left(-0.87 + 17.9\alpha_t^2\right)\alpha_t \tag{2}$$

The same pattern of variation with α_t was also observed for the "BASIC FINNER" projectile and is given in Ref. 12. It is interesting to notice that both cases exhibit a negative value up to $\alpha_t = 12.6$ deg and then become rapidly positive. This measured behavior, was neither observed nor utilized in Ref. 8, which uses a simplistic sixth-order variation with α_t for a six-fin projectile configuration.

Mechanisms for Lock-In

Reference 4 lists three main missile asymmetry categories that can cause lock in. First is configuration asymmetries, such as fin cant manufacturing tolerance, fin damage during launch or in flight, or a bent nose, all of which result in a static trim angle. Also, rocket thrust misalignment with the body axis is another example. Second is the mass center location deviation from the body axis, which provides coupling of the roll with the aerodynamic normal force of the vehicle. Third is the aerodynamic–geometric interactions such as the fin rotation/angle-of-attack interaction causing the induced roll moment described earlier. Elastic bodies that can bend or deform, thus causing a change in the aerodynamic forces from their intended design values, are a second example.

Formulation

Analysis of Price: Rolling Coordinates

Price[4] adapted the equations developed earlier by Nielson for a constant spin case, to accept varying spin rate cases. The equations of Nielson for pitch and yaw angles were written in body-fixed coordinates, i.e., rolling with the body itself. Price then added the roll equation (with the induced roll moment). He also added the terms for the effects of mass offset, moment asymmetry, and rocket thrust misalignment to the three equations. The general nomenclature and coordinates are shown in Fig. 5. The roll motion equation was written by Price as

$$I_x\ddot{\phi} = q \cdot A_{\text{ref}} \cdot d \cdot [C_{l\delta} \cdot \delta + C_{lp}(\dot{\phi}d/V) - C_{li} \cdot \sin(n\bar{\phi}) - (\Delta cg/d) \cdot C_{N\alpha} \cdot \alpha_{\text{trim}} \cdot \sin(\bar{\phi} - \Gamma)] \tag{3}$$

subject to the initial condition

$$\dot{\phi} = \dot{\phi}_0 \qquad \text{at} \qquad t = 0 \tag{4}$$

where

$$\dot{\phi} \equiv \frac{\mathrm{d}\phi}{\mathrm{d}t} = p, \qquad \psi = \tan^{-1}\left[\frac{bp/\omega_p}{1 - p^2(1 - Ix/Iy)/\omega_p^2}\right]$$

$$\bar{\phi} = \lambda - \psi, \qquad b = \left(\frac{q A_{\text{ref}}}{mV\omega_p}\right)\left(C_{N\alpha}\left(1 - \frac{I_x}{I_y}\right) - \frac{md^2 C_{Mq}}{I_y}\right)$$

Also, $-\psi$ is the phase angle, and $\bar{\phi}$ is the fin orientation angle.

Nonrolling Coordinates

The analysis of Ref. 7 is almost standard in ballistics formulation. It uses a ballistic coordinate system, i.e., axes are attached to the c.g. of the body and move with it, but do not roll with the body. Reference 7 has the standard form, which was expanded here in the α, β, and time variables, modified for the added asymmetry effects, and rewritten in Price's form:

$$\ddot{\beta} + A_1\dot{\beta} - A_2\dot{\alpha} - B_1\beta + B_2\alpha = C_1 \tag{5}$$

$$\ddot{\alpha} + A_1\dot{\alpha} + A_2\dot{\beta} - B_1\alpha - B_2\beta = C_2 \tag{6}$$

where

$$A_1 = \left(\frac{q A_{\text{ref}}}{mV}\right)\left(C_{L\alpha} - \frac{md^2}{I_y}(C_{Mq} + C_{M\dot{\alpha}})\right)$$

$$A_2 = -p\left(\frac{I_x}{I_y}\right), \qquad B_1 = \left(\frac{q A_{\text{ref}} d}{I_y}\right)C_{M\alpha}$$

$$B_2 = \left(\frac{pq A_{\text{ref}}}{mV}\right)\left(\frac{C_{L\alpha} I_x}{I_y} + \frac{md^2}{I_y}C_{Mp\alpha}\right)$$

$$C_1 = \left(\frac{q A_{\text{ref}} d}{I_y}\right)\left[C_{M0}\cos(\lambda + \phi) - C_A\left(\frac{\Delta cg}{d}\right)\cos(\Gamma + \phi)\right]$$

$$C_2 = \left(\frac{q A_{\text{ref}} d}{I_y}\right)\left[C_{M0}\sin(\lambda + \phi) - C_A\left(\frac{\Delta cg}{d}\right)\sin(\Gamma + \phi)\right]$$

The λ angle is such that $C_{M0z} = C_{M0}\cos(\lambda)$ and $C_{M0y} = C_{M0}\sin(\lambda)$. The pitch angle α is positive when the vehicle nose is up, whereas C_M (hence, $C_{M\alpha}$) is negative when it turns the nose tip down.

The roll equation [Eq. (3)] is modified for the nonspinning axes and rewritten after Price's model as

$$I_x\ddot{\phi} = q \cdot A_{\text{ref}} \cdot d \cdot [C_{l\delta} \cdot \delta + C_{lp}(\dot{\phi}d/V) - C_{li} \cdot \sin(n\bar{\phi}) - (\Delta cg/d) \cdot C_{N\alpha} \cdot \alpha_t \cdot \sin(\phi + \Gamma - \hat{\phi})] \tag{7}$$

where $\bar{\phi}$ is the angle between the pitch plane and the fin orientation plane. The velocity along the trajectory, V, is numerically computed using Newton's equation along the trajectory, the muzzle launch velocity, and the drag coefficient (which is function of Mach number). Also, the yaw angle amplification factor (AMP) is expressed as[13]

$$\text{AMP} = \frac{\alpha_t}{\alpha_{\text{trim at zero spin}}} = \frac{-0.5\rho A_{\text{ref}} d C_{M\alpha}}{I_y\sqrt{\left\{[(\bar{p} - \dot{\phi}_f)(\bar{p} - \dot{\phi}_s) - \lambda_f\lambda_s]^2 + [\lambda_s(\bar{p} - \dot{\phi}_f) + \lambda_f(\bar{p} - \dot{\phi}_s)]^2\right\}}}$$

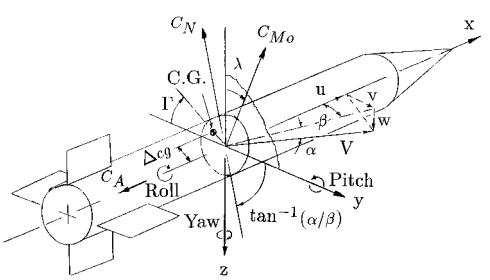

Fig. 5 Nomenclature, coordinates, and angles (after Price[4]).

where

$$\bar{p} = p/V, \qquad \dot{\phi}_f = \frac{\bar{p} I_x(1 + \sigma)}{(2I_y)}, \qquad \dot{\phi}_s = \frac{\bar{p} I_x(1 - \sigma)}{(2I_y)}$$

$$\sigma = \sqrt{1 - \frac{1}{S_g}}, \qquad S_g = \frac{2I_x^2\bar{p}^2}{(\pi I_y \rho C_{M\alpha} d^3)}$$

$$\lambda_f = \frac{\rho A_{\text{ref}}}{4m}\left[-C_{N\alpha}\left(1 - \frac{1}{\sigma}\right) + 0.5k_2\left(1 + \frac{1}{\sigma}\right)C_{Mq} + \frac{k_1 C_{Mp\alpha}}{\sigma}\right]$$

$$\lambda_s = \frac{\rho A_{\text{ref}}}{4m}\left[-C_{N\alpha}\left(1+\frac{1}{\sigma}\right)+0.5k_2\left(1-\frac{1}{\sigma}\right)C_{Mq}-\frac{k_1 C_{Mp\alpha}}{\sigma}\right]$$

$$k_1 = \frac{md^2}{I_x}, \qquad k_2 = \frac{md^2}{I_y}$$

Fin Damage

In ballistics practice, damage to fins may be observed on x-ray or video films taken for projectiles coming out of the muzzle. Some fin damage is only realized when yaw tests (using yaw cards) are performed. However, fin damage cannot be predicted a priori. Most fin damage occurs in the gun tube and before exiting the muzzle. (Some damage due to aeroheating may occur during flight.) Seldom are the fins recovered after each firing to examine the damage. In many cases fin damage could only be assumed, based on untypical flight performance such as large yaw angles at large ranges (3000–10,000 ft for projectile applications) or a screen impact imprint indicating rod bending or even missing or bent fins. Unfortunately, for those observed flight abnormalities, no fin damage was expected nor were the fins recovered. Therefore, theoretical studies and models, like the present work, are used to explain the relation between the abnormal flight behavior, e.g., roll/pitch lock-in or roll/flexure lock-in, and possible fin damage. A question is often posed about how much and what type of fin damage it takes to cause such behavior, even if the damage itself cannot be prevented. The present work sheds some light in that respect. Theoreticians assign numerical values to asymmetries but they never relate these to real-life fin damage and examine if those values were realistic.[8]

In the present study, fin damage is idealized into three types that are most often observed from yaw card tests. Corresponding damaged fin areas of 5% and 10% for a single fin panel bent at different damage angles are studied as a practical example. The fin damage cannot be just arbitrarily assumed in size and direction, but must be made consistent to explain the loss in roll rate from its design value as well. Therefore, only damages in a certain direction relative to the fin cant angle and spin direction can be applied. Although other fin angle damage directions obviously happen, they will not result in lower roll and, thus, in this spin/pitch lock-in. In fact, Ref. 10 purposefully considered the reverse case only, i.e., only damage that will overspin the projectile, to study the spin/flexure lock-in behavior. Figure 6 shows the required fin damage direction to cause a change in fin normal force and roll moment for an equivalent fin panel canted at δ_{eq}. The projectile roll is positive when counterclockwise (looking forward from the tail), and δ_{eq} is positive when it is up in the direction of producing positive roll. The static (nonrolling) asymmetries ΔC_N and ΔC_M (C_{M0}) can be positive or negative, depending on the damage location and direction. Further details will be discussed in the Case Study section.

Mass Offset

The projectile mass asymmetry is represented by the mass offset radial distance Δcg. This offset, which always exist in real life with different degree of severity, creates a rolling moment due to the normal force, which acts on the geometric, not the mass center point of the rod cross section. This offset also gives rise to a pitching and yawing moments due to the aerodynamic axial force C_A, as can be seen in Fig. 5 and is reflected in Eqs. (5) and (6).

A value of $\Delta cg = 0.20d$ is extremely large and has been used only as an application example. Actual practical values are of the order of 0.003–$0.009d$ for projectile applications. For missile applications, this offset is usually larger than those given for projectiles.

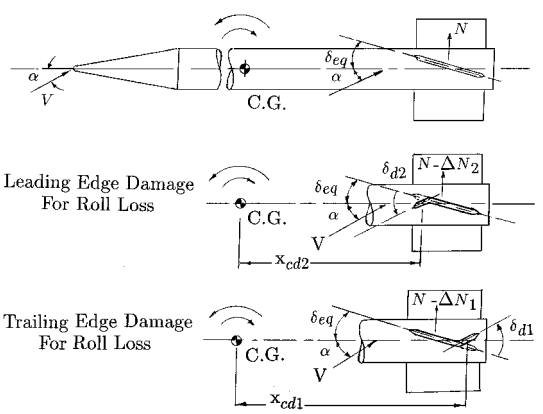

Fig. 6 Leading- and trailing-edge idealized fin damage.

Case Study

Calculations were performed to simulate the case of a subcaliber projectile that has an L/d of 22.72, as given in Fig. 2. The aerodynamic coefficients were obtained from the U.S. Army Ballistic Research Laboratory enclosed transonic range test database. In the enclosed range the tests are made on steel models rather than on the actual rounds for safety considerations. Therefore, simulations were also made for that particular case. The relevant information regarding this configuration is given in Table 1.

Computations were performed for 23 cases with four different steady-state spin values, covering the spectra of above/at/below the pitching frequency case. The pitching frequency was 25 Hz at launch ($M = 5$) and drops to 23 Hz at Mach $= 4.0$ (or about $t = 0.9$ s). The different steady-state spin cases were considered to reflect the effect of damaged fins. The actual equivalent fin cant angle for the projectile is 0.55 deg, resulting in a steady-state spin of 90 Hz. Table 2 provides the fin cant angle values applied to simulate damaged fins and the corresponding steady-state spin values. These chosen spin values were selected so as to provide insight about resonance behavior near and through the pitching frequency ω_p.

For quantified fin damage, three idealized types were modeled reflecting leading-, trailing-, and tip-edge damage, as shown in Fig. 7

Table 1 Physical properties of the projectile

Ref. diameter	1.06 in.
L/d	22.72
Material	Steel
Mass	4.281 lb
I_x	0.6956 lb-in.^{2}
I_y	143.56 lb-in.^{2}
Launch speed	5905.8 ft/s
Launch spin	0 Hz

Table 2 Equivalent fin cant and steady-state spin

Case no.	Fin status	Equivalent fin cant angle, deg	Cant angle as fraction of δ_d	Steady-state spin, Hz
I	Undamaged	0.55	$(1.0\delta_d)$	90
IIa	Damaged	0.22	$(0.4\delta_d)$	36
IIb	Damaged (spin above ω_p)	0.165	$(0.3\delta_d)$	27
III	Damaged (spin at ω_p)	0.137	$(0.25\delta_d)$	22.5
IV	Damaged (spin below ω_p)	0.11	$(0.2\delta_d)$	18

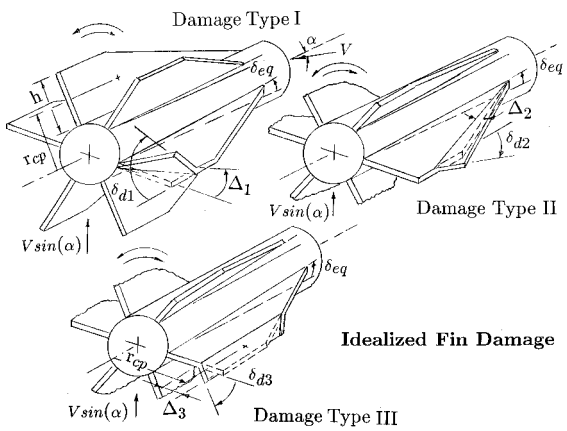

Fig. 7 Three types of idealized fin damage.

Table 3 Damaged fin areas and angles with their corresponding ΔC_N and ΔC_M

Resulting reduced roll rate, Hz	Uniform damage to six fins			Equivalent damage to a single fin			Single fin damage parameters and forces								
							Damage type I		Damage type II		Damage type III			$\Delta C_M (\equiv C_{M0})$ Damage type	
	Initial δ_{eq}, deg	δ_{dg}, deg	Final δ_{eq}, deg	δ_{dg}, whole panel, deg	Damaged area (A_d/A_f)	δ_{dg}, deg	Δ_1, deg	δ_1, deg	Δ_2, deg	δ_2, deg	Δ_3, in.	δ_3, deg	ΔC_N $(\equiv C_{N0})$	I	II	III
36	0.55	−0.33	0.22	−1.43	0.05	−28.6	16	+28.6	1.5	−28.6	0.07h	−28.6	−0.094	+0.97	+0.78	+0.93
					0.10	−14.3	30	+14.3	3.0	−14.3	0.16h	−14.3				
27	0.55	−0.385	0.165	−1.76	0.05	−35.2	16	+35.2	1.5	−35.2	0.07h	−35.2	−0.116	+1.20	+0.96	+1.15
					0.10	−17.6	30	+17.6	3.0	−17.6	0.16h	−17.6				
22.5	0.55	−0.412	0.138	−1.92	0.05	−38.4	16	+38.4	1.5	−38.4	0.07h	−38.4	−0.126	+1.31	+1.04	+1.25
					0.10	−19.2	30	+19.2	3.0	−19.2	0.16h	−19.2				
18	0.55	−0.44	0.11	−2.09	0.05	−41.8	16	+41.8	1.5	−41.8	0.07h	−41.8	−0.137	+1.42	+1.14	+1.36
					0.10	−20.9	30	+20.9	3.0	−20.9	0.16h	−20.9				

Table 4 Independent mass offset and asymmetry moment values used

Mass offset, $\Delta cg/d$	C_{M0}	Corresponding trim angle for C_{M0}, deg
0.0	0.0	0.0
0.001	+0.061	−0.1
0.004	+0.122	−0.2
0.01	+0.305	−0.5
0.04	+0.428	−0.7
0.08	+0.489	−0.8
0.10	+0.916	−1.5
0.12	+1.222	−2.0
0.20	+2.444	−4.0

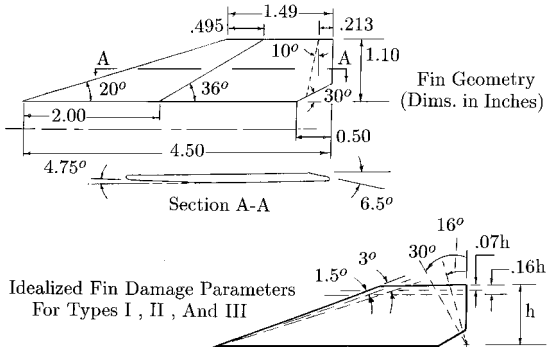

Fig. 8 Quantified fin area damage for types I, II, and III.

for the six-fin configuration. The actual fin shown in Fig. 8 is modeled by an equivalent fin wholly canted at $\delta_{eq} = 0.55$ deg. Representative damage area for the three types are also shown in Fig. 8. The corresponding change in normal force and C_M were computed and are presented in Table 3. An idealized equivalent uniform fin cant angle damage for the six fins is listed. A single panel with a damaged area equivalent bend angle is modeled to provide the same lower spin rate that the six damaged fins would have. The corresponding change in the fin normal force ΔC_N and the corresponding change in C_M, i.e., C_{M0}, were then computed. The corresponding values for damages type I, II, and III are all listed in Table 3. The $C_{N\alpha}$ of the fin set, including its body interference effect, was computed by using the NSWC-AP95 fast design code.[14] Linear aerodynamics was used to provide engineering estimates for the fin damage angles in association with the damaged fin panel areas. For example, a 5% area fin damage bent at 8 deg would be equivalent to a 10% fin area damage bent at 4 deg. Although this linearity may not be valid for large angles, it simplifies the procedure. More sophisticated nonlinear models may obviously be devised.

Different independent values for the mass offset were used, ranging between $0.0d$ and $0.20d$. $C_{M\alpha}$ for the undamaged projectile was −35 at the launch speed. Values for C_{M0} varying between 0.0 and +2.444 (corresponding to 0.0- and −4.0-deg static trim angle) were used. The exact values used for both parameters are listed in Table 4.

Computations

Computations were made by solving the three equations as an initial value problem. The alpha and beta equations were solved simultaneously, followed by the roll equation. Small time steps were used ($\Delta t = 9.0 \times 10^{-6}$ s). Three-point, central differences, second-order accurate (in time) finite differencing was used, with recurrence relations relating the variable value at the $n+1$ time level to the previous n and $n-1$ time levels. Knowing the first two values at time zero and at Δt using the initial conditions, one can then proceed directly.

The roll equation was solved as a first-order equation in $\dot{\phi}$, with the initial condition given by Eq. (4). Equation (3) was written as

$$I_x(\ddot{\phi})_n + BB|_n\dot{\phi}_n + CC|_n = 0 \tag{8}$$

The solution was then computed as

$$\dot{\phi}_{n+1} = \dot{\phi}_n - \Delta t\frac{BB|_n\dot{\phi}_n + CC|_n}{I_x} \tag{9}$$

The roll equation is coupled to the pitch/yaw equations through the induced roll moment term, which includes α_t and C_{li}.

Calculations were usually stopped at about $t = 0.9$ s, which corresponds, for the case considered, to a distance of about 5578 ft down from the gun muzzle. This corresponds to about 300,000 time steps. A single case takes about 15 s on a Unix SGI minicomputer (workstation).

Results

Because of the many parameters of the problem, one set of similar conditions was applied so that the spin/pitch lock-in phenomenon can be observed without changing the parameters. Later studies may be made with these parameters as variables to discuss their individual influences in detail.

The initial conditions, for example, were held the same for all cases. The values $\alpha(t_0) = 4$ deg, $\beta(t_0) = 3$ deg, $\dot{\alpha}(t_0) = 1.0$ rad/s, and $\dot{\beta}(t_0) = 1.0$ rad/s were used.[15] The roll equation was also solved under zero initial values for both ϕ and $\dot{\phi}$. Any other values may obviously be prescribed for other desired conditions.

Other parameters are the mass offset initial location angle Γ and the C_{M0} moment orientation angle λ. They were taken to be 30 and 70 deg, respectively. Reference 4 provides a discussion about the λ angle role in the lock-in. A list of cases computed in this study and the corresponding values of the parameters used are provided in the form of Table 5.

First, the case of spinning above ω_p with steady-state spin of 36 Hz is presented. The case with no fin damage or asymmetries was computed, and the typical α- and β-angle histories are given in Fig. 9, both approaching zero values at about $t = 0.6$ s, approximately.

Cases 2–10 were computed with varying Δcg but with zero C_{M0}. For the higher spin rate of 36 and 27 Hz, no lock in occurred with the given values of Δcg, as shown in Figs. 10 and 11, respectively. Although the value $0.20d$ is relatively large and is not expected in practice, one must remember that no C_{M0} was applied here, which is not the case in real life. However, as the steady-state spin due to damage gets closer to the pitch frequency, such as for the cases of 22.5 and 18 Hz, lock-in occurs with a smaller values of Δcg.

Table 5 Cases computed and parameter values

Case no.	Equivalent fin cant angle	C_{M0}	C_{M0} corresponding trim angle, deg	$\Delta cg/d$	Lock-in status
1	$0.4\delta_d$	0.0	0.0	0.04	No lock
2	$0.4\delta_d$	0.0	0.0	0.08	No lock
3	$0.4\delta_d$	0.0	0.0	0.20	No lock
4	$0.3\delta_d$	0.0	0.0	0.0	No lock
5	$0.3\delta_d$	0.0	0.0	0.04	No lock
6	$0.3\delta_d$	0.0	0.0	0.12	No lock
7	$0.25\delta_d$	0.0	0.0	0.0	No lock
8	$0.25\delta_d$	0.0	0.0	0.08	Lock-in
9	$0.2\delta_d$	0.0	0.0	0.0	No lock
10	$0.2\delta_d$	0.0	0.0	0.10	Lock-in
11	$0.4\delta_d$	+0.305	−0.5	0.0	Lock-in
12	$0.4\delta_d$	+0.916	−1.5	0.0	Lock-in
13	$0.4\delta_d$	+2.444	−4.0	0.0	Lock-in
14	$0.3\delta_d$	0.0	0.0	0.0	No lock
15	$0.3\delta_d$	+0.428	−0.7	0.0	Lock-in
16	$0.3\delta_d$	+1.222	−2.0	0.0	Lock-in
17	$0.25\delta_d$	0.0	0.0	0.0	No lock
18	$0.25\delta_d$	+0.061	−0.2	0.0	Lock-in
19	$0.2\delta_d$	0.0	0.0	0.0	No lock
20	$0.2\delta_d$	+0.610	−2.0	0.0	Lock-in
21	$0.4\delta_d$	+0.061	−0.10	0.001	No lock
22	$0.4\delta_d$	+0.122	−0.20	0.040	No lock
23	$0.4\delta_d$	+0.489	−0.80	0.100	Lock-in

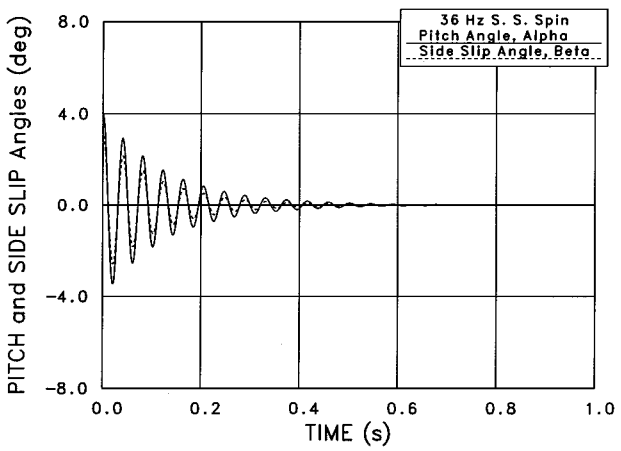

Fig. 9 Pitch and side-slip angles for no lock-in case: $\delta_{eq} = 0.4\delta_d$, $C_{M0} = 0.0$, and $\Delta cg = 0.0$; for 120-mm M829 KE projectile (steel).

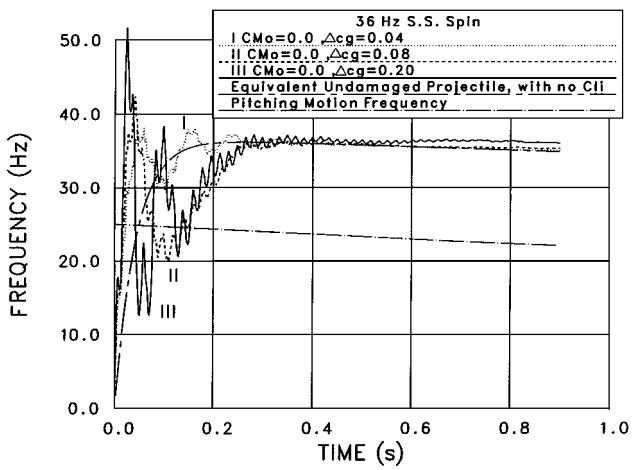

Fig. 10 Roll/pitch resonance and then escaping pitch lock-in: $\delta_{eq} = 0.4\delta_d$, $C_{M0} = 0.0$, and increasing Δcg; for 120-mm M829 KE projectile (steel).

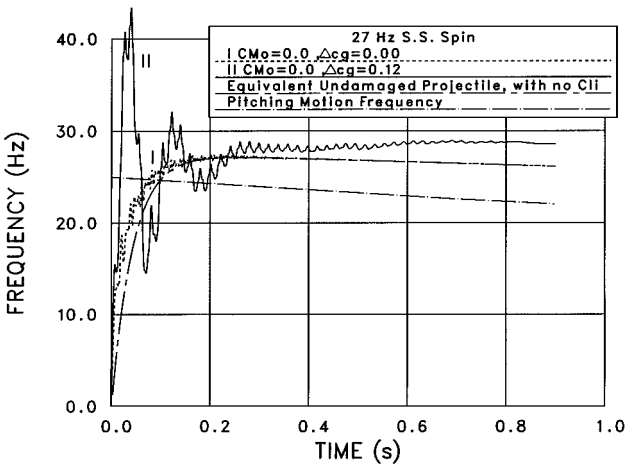

Fig. 11 Roll/pitch resonance and then escaping pitch lock-in: $\delta_{eq} = 0.3\delta_d$, $C_{M0} = 0.0$, and increasing Δcg; for 120-mm M829 KE projectile (steel).

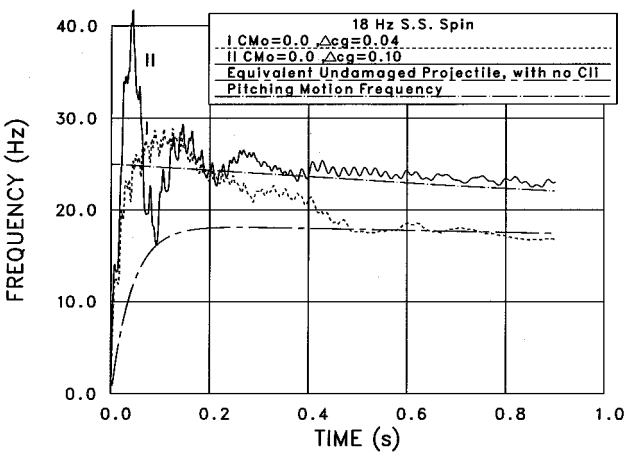

Fig. 12 Roll/pitch resonance and roll/pitch lock-in: $\delta_{eq} = 0.2\delta_d$, $C_{M0} = 0.0$, and increasing Δcg; for 120-mm M829 KE projectile (steel).

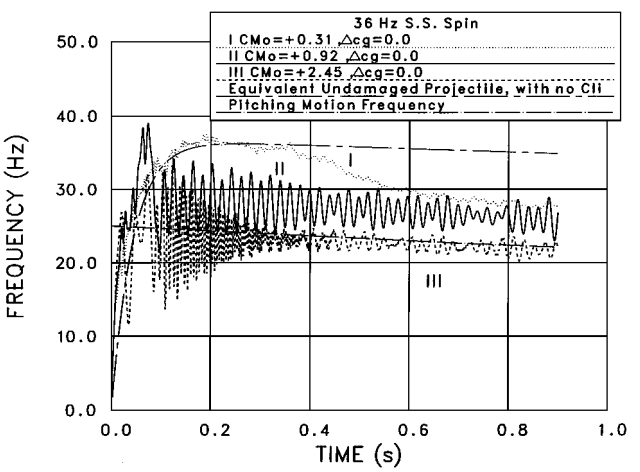

Fig. 13 Roll/pitch lock-in: $\delta_{eq} = 0.4\delta_d$, increasing C_{M0}, and $\Delta cg = 0.0$; for 120-mm M829 KE projectile (steel).

Figure 12 indicates the lock-in for the 18 Hz case after about 0.5 s from launch.

Cases 11–20 examine the effect of increasing the value of C_{M0} without the mass offset influence being present. Figure 13 shows the effect of increasing C_{M0} for the fin damage spin of 36 Hz. Interesting to note that, for smaller fin damage, it takes longer time to lock-in, whereas for larger damage lock-in occurs faster and with closer value to the pitch frequency. The same behavior is shown in Fig. 14 for the fin damage of 27-Hz steady-state spin. Figure 15 shows the

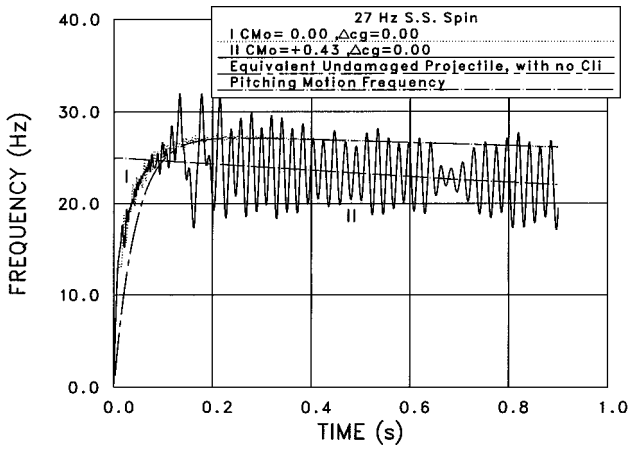

Fig. 14 Roll/pitch lock-in and no lock-in: $\delta_{eq} = 0.3\delta_d$, increasing C_{M0}, and $\Delta cg = 0.0$; for 120-mm M829 KE projectile (steel).

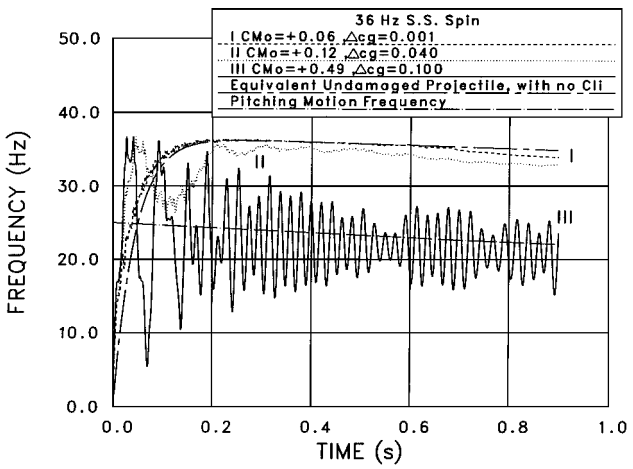

Fig. 15 Roll resonance and roll/pitch lock-in: $\delta_{eq} = 0.4\delta_d$, and increasing both C_{M0} and Δcg; for 120-mm M829 KE projectile (steel).

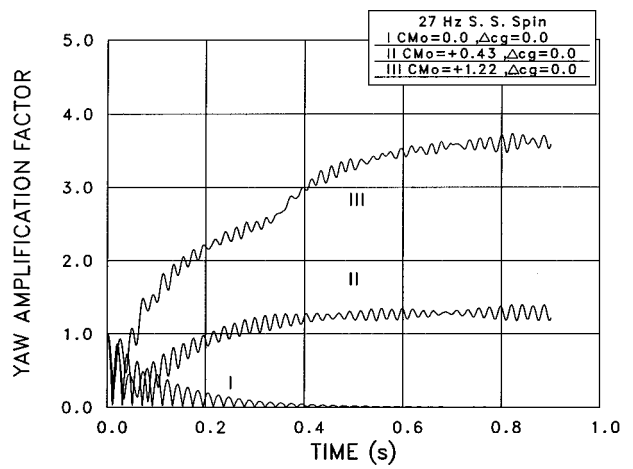

Fig. 16 Yaw angle amplification for roll/pitch lock-in: $\delta_{eq} = 0.3\delta_d$, increasing C_{M0}, and $\Delta cg = 0.0$; for 120-mm M829 KE projectile (steel).

yaw angle amplification factor for this later case. The amplification factor is defined here as the computed trial angle of attack devided by the initial total angle of attack. Amplification factors of 1.2 and 3.6 are noticed for cases with fin damage, whereas attenuation to a value of zero is noticed for the case with no fin damage.

In real-life cases, usually both asymmetries and mass offset occur. Cases 21–23 were computed showing increased values for both parameters. Pitch resonance changes to pitch lock-in when both parameters were increased as reflected by cases 21–23 of Table 5 and shown in Fig. 16. Figure 16 shows the change from short-lived pitch resonance to full lock-in with ω_p when the asymmetry damage increased. Figure 17 shows the α- and β-angle histories for case 21, which reflects very small asymmetries. The plot indicates almost unaffected motion.

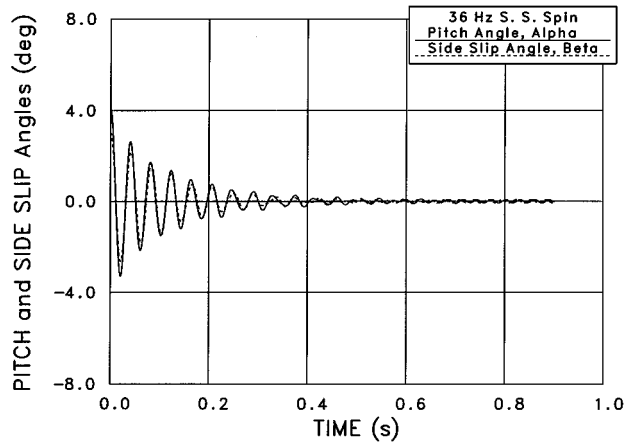

Fig. 17 Pitch and side-slip angles for a case of very slight asymmetries: $\delta_{eq} = 0.4\delta_d$, $C_{M0} = +0.061$, and $\Delta cg = 0.001$; for 120-mm M829 KE projectile (steel).

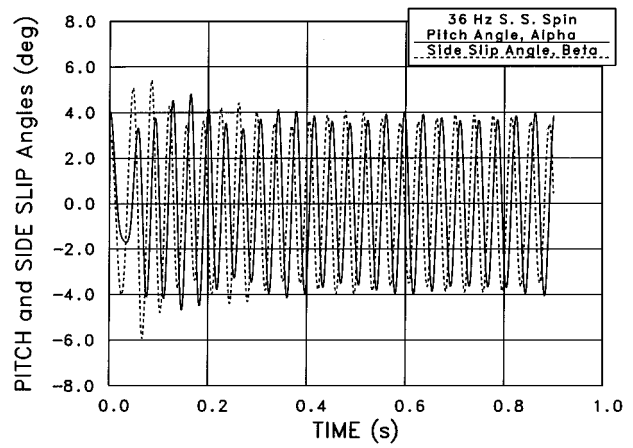

Fig. 18 Pitch and side-slip angles for case of roll/pitch lock-in: $\delta_{eq} = 0.4\delta_d$, $C_{M0} = +0.916$, and $\Delta cg = 0.0$; for 120-mm M829 KE projectile (steel).

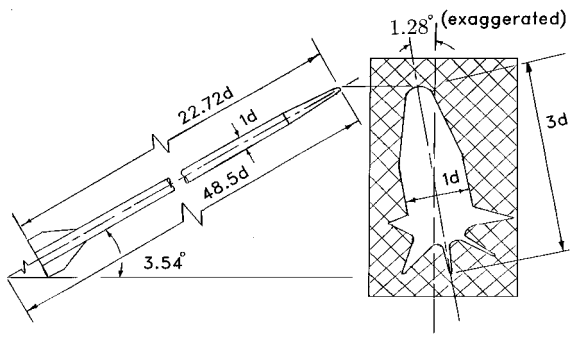

Fig. 19 Predicted impact imprint of a case of roll/pitch lock-in: $\delta_{eq} = 0.4\delta_d$, $C_{M0} = +0.916$, and $\Delta cg = 0.0$; at $x = 1189.73$ m and $t = .6935$ s.

The expected impact imprint on cardboard yaw cards (or wire mesh screens) used in measuring the yaw motion in practical ballistics can now be constructed from the results computed. Figure 18 presents the α- and β-angle histories for case 12 for lock-in. Figure 19 shows the expected imprint for the lock-in case of Fig. 18 at $t = 0.633$ s, where $\|\alpha\|$ and $\|\beta\|$ were computed to be 3.54 and 1.28 deg, respectively, with a total yaw angle of 3.76 deg. A harsher case of lock-in with a larger C_{M0} is shown in Figs. 20 and 21. The $\|\alpha\|$ and $\|\beta\|$ computed were 9.44 and 5.60 deg, respectively, thus, yielding a total yaw angle of 11.97 deg at $t = 0.194$ s.

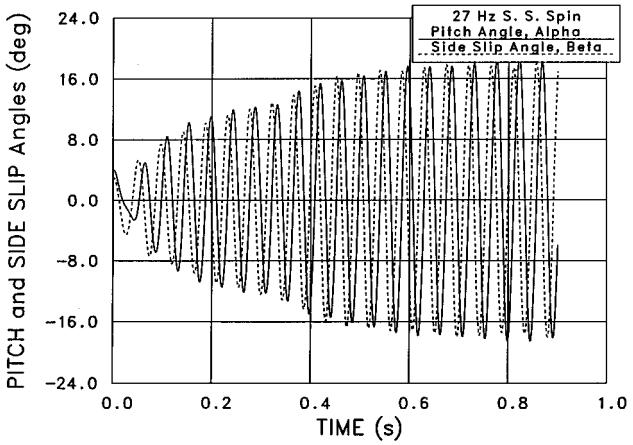

Fig. 20 Pitch and side-slip angles for a case of roll/pitch lock-in: δ_{eq} = $0.3\delta_d$, C_{M0} = +1.222, and Δcg = 0.0; for 120-mm M829 KE projectile (steel).

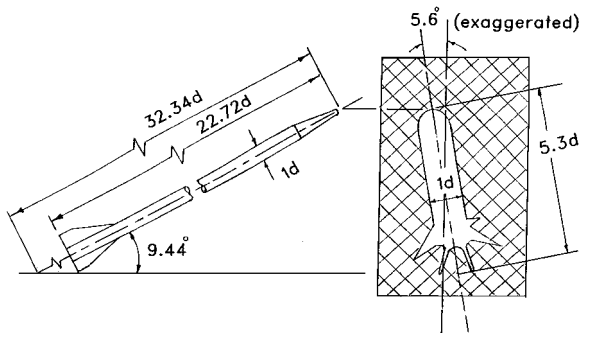

Fig. 21 Predicted impact imprint of a case of roll/pitch lock-in: δ_{eq} = $0.3\delta_d$, C_{M0} = +1.222, and Δcg = 0.0; at x = 344.86 m and t = 0.1942 s.

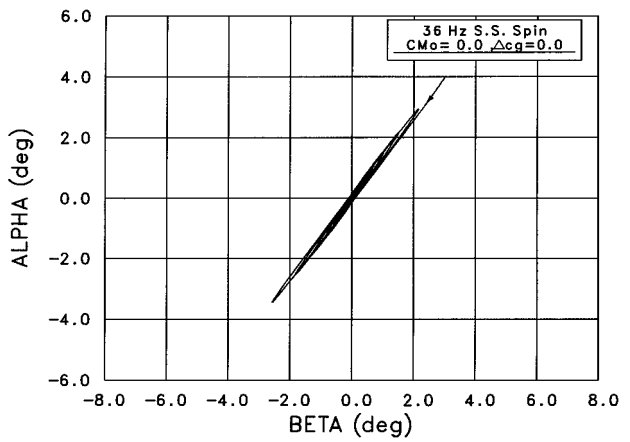

Fig. 22 No lock-in case α–β plot: δ_{eq} = $0.4\delta_d$, C_{M0} = 0.0, and Δcg = 0.0; for 120-mm M829 KE projectile (steel).

In the practice of ballistics, the α–β plot is usually monitored to provide insight into the flight. The three cases of no lock-in, late lock-in, and immediate lock-in are presented in Figs. 22–24. Figure 22 provides the typical KE flight pattern with no asymmetry and, therefore, no lock-in. Figure 23 shows case 11, which locked in later in its flight, as was also indicated by curve 1 of Fig. 13. Figure 24 shows the case of a quick roll/pitch lock-in of case 23. As can be seen, all cases started with the same initial conditions of $\alpha = 3$ deg and $\beta = 4$ deg.

Additional cases can now be routinely computed. Reference 4 provides a simple guideline for the expected values for both asymmetry parameters for lock-in. These values may be used as first estimate for the value of the parameter under which the vehicle may lock-in. The exact value can then be determined by computing the case with perturbations on these estimates and monitoring the resulting spin history, and the α–β plot.

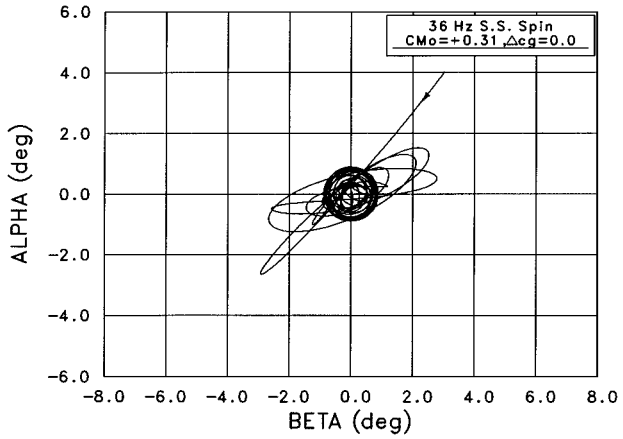

Fig. 23 Case with roll resonance and later roll/pitch lock-in α–β plot: δ_{eq} = $0.4\delta_d$, C_{M0} = +0.305, and Δcg = 0.0; for 120-mm M829 KE projectile (steel).

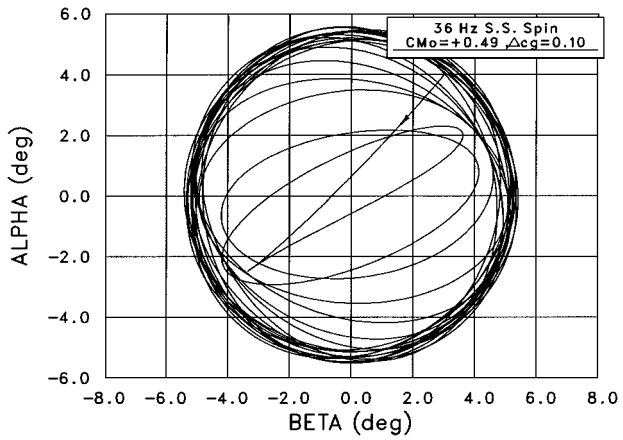

Fig. 24 Lock-in case α–β plot: δ_{eq} = $0.4\delta_d$, C_{M0} = +0.489, and Δcg = $0.10d$; for 120-mm M829 KE projectile (steel).

Conclusions

Trajectory cases for the given projectile of Fig. 2 were computed for the 23 cases listed. Straightforward application of the model was achieved with no difficulties. The spin response was monitored for all fin damage and mass offset cases. The very short time of the computations enabled the running of many other cases, which are not listed in this work, to examine the sensitivity of the spin response to the magnitude of each of the mass offset and the fin damage and the combination of them.

The following conclusions are supported by the results obtained through the application of the present analysis and model.

1) Fin area damage, in certain size and direction, can cause the lowering of the design steady-state spin to a value close to the vehicle pitching motion frequency, thus creating the environment for possible locking in to that frequency.

2) It does not take large fin damage to cause the low spin and, therefore, providing the condition for possible locking in with the pitching motion frequency. For the case studied for a six-finner, a single fin panel idealized area damage of 10% of the fin area, bent at 19.2 deg, was enough to lower the spin and also cause the lock-in.

3) The higher or lower the expected steady-state spin (due to damage) differs from the pitching motion frequency, the larger the mass offset is needed to cause lock-in, in absence of fin asymmetry damage.

4) If the fin damage is less than that required to cause lock-in, the spinning motion will escape from being locked in but with some resonance effect on the spin history.

5) In case of mass offset alone, lock-in can also theoretically happen with no moment asymmetries ($C_{M0} = 0.0$).

6) If a combination of both asymmetry moment and mass offset is causing the lock-in, their individual required magnitudes will be

less than those required if each were to have been applied alone to cause a lock-in (confirming one's expectation).

In summary, a model was developed to study and simulate the roll and pitching motions lock-in observed for some projectiles in flight. Fin damage and mass offset were quantified, and their effects on the motion of the vehicle were computed. Flight histories of the motion including the spin rate, pitch and yaw angles, and yaw amplification factor are computed. Both roll resonance and roll lock-in behavior were reflected in the flight histories computed. Projectile impact imprint on yaw cards is predicted and simulated for any distance from the muzzle. The model established is general for missile or finned projectile applications. A case study was performed in detail for a specific projectile, as a real-life applied example.

References

[1]Pennekamp, R. A., and Jara, E. A., "M900 Technical Test Results: Yaw and Spin Characterization Subtest," U.S. Army Ballistic Research Lab., BRL-MR-3941, Aberdeen Proving Ground, MD, Dec. 1991.

[2]Pennekamp, R. A., "M829A2 Technical Test Results: Yaw and Spin Characterization Subtest," U.S. Army Research Lab., ARL-MR-46, Aberdeen Proving Ground, MD, Feb. 1993.

[3]Nicolaides, J. D., "On the Free Flight Motion of Missile Having Slight Configurational Asymmetries," U.S. Army Ballistic Research Lab., BRL-Rept. 858, Aberdeen Proving Ground, MD, June 1953; also Inst. of Aeronautical Sciences Paper 395, Jan. 1953.

[4]Price, D. A., Jr., "Sources, Mechanisms and Control of Roll Resonance for Sounding Rockets," *Journal of Spacecraft and Rockets*, Vol. 4, No. 11, 1967, pp. 1516–1525.

[5]Clare, T. A., "Non-Linear Resonance Instability in the Flight Dynamics of Missiles," Ph.D. Dissertation, Dept. of Aerospace and Mechanical Engineering, Univ. of Notre Dame, Notre Dame, IN, June 1970.

[6]Clare, T. A., "Resonance Instability for Finned Configurations Having Nonlinear Aerodynamic Properties," *Journal of Spacecraft and Rockets*, Vol. 8, No. 3, 1971, pp. 278–283.

[7]Murphy, C. H., "Free Flight Motion of Symmetric Missiles," U.S. Army Ballistic Research Lab., BRL Rept. 1216, Aberdeen Proving Ground, MD, July 1963.

[8]Murphy, C. H., "Some Special Cases of Spin-Yaw Lock-In," *Journal of Guidance, Control, and Dynamics*, Vol. 12, No. 6, 1989, pp. 771–776.

[9]Lin, T. C., Sproul, L. K., and Muskat, R., "Persistent Roll Resonance Induced by Missile/RV Aeroelastic Behavior," AIAA Paper 95-0065, Jan. 1995.

[10]Mikhail, A. G., "In-Flight Flexure and Spin Lock-In for Kinetic Energy Projectiles," *Journal of Spacecraft and Rockets*, Vol. 33, No. 5, 1996, pp. 657–664.

[11]Legner, H. H., Lo, E. Y., and Reinecke, W. G., "Hypervelocity Projectile Design Implications at High Fineness Ratio," AIAA Paper 95-0064, Jan. 1995.

[12]Oberkampf, W. L., and Nicolaides, J. D., "Aerodynamics of Finned Missiles at High Angle of Attack," *AIAA Journal*, Vol. 9, No. 12, 1971, pp. 2378–2384.

[13]Arrow Tech Associates, "User Manual—PC PRODAS Code, Version 3.6," Arrow Tech Co., South Burlington, VT, 1991.

[14]Moore, F. G., Hymer, T. C., and McInville, R. M., "The 1995 Version of the NSWCDD Aeroprediction Code: Part II—Computer Program User's Guide and Listing," U.S. Naval Surface Warfare Center, NSWCDD/TR-95/5, Dahlgren Div., Dahlgren, VA, March 1995.

[15]Erline, T. F., "Lateral Projectile Dynamics: M829 Projectile—Style vs. Puller Sabot," U.S. Army Research Lab., ARL-TR-630, Aberdeen Proving Ground, MD, Nov. 1994.

J. R. Maus
Associate Editor